



Spatiotemporal denudation rates of the Swabian Alb escarpment (Southwest Germany) dominated by base-level lowering and lithology

Mirjam Schaller^{1,2}, Daniel Peifer¹, Alexander B. Neely¹, Thomas Bernard¹, Christoph Glotzbach¹,
5 Alexander R. Beer¹, Todd A. Ehlers²

¹Department of Geosciences, University of Tuebingen, 72076 Tuebingen, Germany

²School of Geographical and Earth Sciences, University of Glasgow, Glasgow, United Kingdom

Correspondence to: Mirjam Schaller (mirjam.schaller@glasgow.ac.uk)

10 **Abstract.** Surface denudation rates, a composite of physical erosion and chemical weathering, are governed by the tectonic, lithologic, climatic, and biotic conditions of a landscape. Disentangling and quantifying these rates is challenging but important for understanding and predicting landscape evolution over space and time. In this study, we focus on a low-relief and mixed lithology mountain range (Swabian Alb escarpment, Southwest Germany), whose 200 to 400 m high escarpment front and foreland drain into the Neckar River to the north and whose plateau drains into the Danube River to the southeast. These two 15 drainage systems are subjected to similar uplift rates and climate/biota but incorporate different lithologies and have different base-levels and topography. We calculate decadal-scale chemical weathering and physical erosion rates based on 30 locations with suspended and dissolved river load measurements and compare them to published longer-term rates to evaluate how these differences influence landscape evolution.

Chemical weathering rates (based on the dissolved river load and corrected for anthropogenic input) range from 0.009 to 0.082 20 mm/yr, while physical erosion rates (calculated from suspended river load and discharge) range from 0.001 to 0.072 mm/yr. The catchment-wide denudation rates range from 0.005 to 0.137 mm/yr, resulting in chemical depletion fractions between 0.48 and almost 0.99. These high values indicate that chemical weathering is generally the dominant erosion process in this cool to temperate, humid mountain range dominated by chemical sedimentary rocks. Both physical erosion and chemical weathering 25 rates are higher in tributaries draining towards the North/Neckar River than in rivers draining towards the Southeast/Danube River, resulting in southeast escarpment retreat rates of 1.2 to 9.3 mm/yr.

Results indicate that the evolution of the Swabian Alb and its escarpment is dominated by base-level lowering and lithology. Decadal-scale denudation rates based on river load may provide insights into the evolution of the escarpment over million-year timescales. The chemical depletion fractions CDFs of the Swabian Alb are compared to other study areas in different 30 tectonic, lithologic, and climatic settings with CDFs ranging from 0.1 to 1.0. We interpret the high CDF values of > 0.5 in the Swabian Alb to result from high chemical weathering rates of the recently exposed lithologies, continuously brought to the surface as a product of late-Cenozoic base-level lowering and consequent south to southeast-directed escarpment retreat across southern Germany. Differences in chemical weathering and physical erosion rates across the escarpment divide may arise from



either the contrast in topographic relief, or exposure of bedrock units that are more susceptible to chemical weathering and physical erosion.

35 1 Introduction

Landscape denudation rates are influenced by tectonics, lithology, climate, and the biota. The process of denudation itself is a composite of physical erosion and chemical weathering by biotic and abiotic processes (e.g., Dietrich and Perron, 2006; Schaller and Ehlers, 2022). Understanding, disentangling, and quantifying rates of these processes across different spatiotemporal resolutions is challenging due to the intricate interplay of the previous factors and the limitations of measurement techniques. However, rates integrating over different timescales can be used to address a broad suite of connections among denudation, short-term human impact and land use, and long-term geological processes including active tectonics and ecosystem dynamics (e.g., Hewawasam et al., 2003; Vanacker et al., 2007; Kirby & Whipple, 2012). Furthermore, rates are needed to calibrate landscape evolution models that seek to simulate Earth surface processes over space and time (e.g., Tucker, 2009). These models can be coupled to better understand the geologic CO₂ budget and its influence on global climate (e.g., Raymo et al., 1988; Maher and Chamberlain, 2014; Bufe et al., 2024).

Disentangling these surface changes can be achieved through several methods (e.g., Gaillardet et al., 1999; Riebe et al., 2004; von Blanckenburg et al., 2012). Most commonly, decadal-scale catchment-wide denudation rates (D ; Figure 1A and B, left side) can be determined by making use of river discharge (Q) and total suspended and dissolved solids (TSS and TDS, respectively), allowing the determination of physical erosion (E) and chemical weathering rates (W ; e.g., Gaillardet et al., 1999; Meybeck, 1986). The rates based on river load include deep weathering but are problematic for capturing bedload transport and sediment transport during infrequent but large magnitude events (e.g., Turowski et al., 2010). Over longer timescales, millennial-scale catchment-wide denudation rates (D) for granitoid lithologies (Figure 1A and B, right side) are determined with in situ-produced cosmogenic ¹⁰Be in river sand (e.g., Brown et al., 1995; Granger et al., 1996). Combining these rates with measurements from immobile elements in soil and bedrock allows the partitioning into physical erosion and chemical weathering rates (Riebe et al., 2004). This partitioning is further used to determine the contribution of chemical weathering to total denudation rate (i.e., the Chemical depletion fraction CDF; Riebe et al., 2004). CDFs range from 0 to 1 reflecting total denudation being completely governed by physical erosion (CDF = 0) or chemical weathering (CDF = 1). Due to deep weathering (e.g., Dixon et al., 2009), immobile elements need to be determined in the soil, saprolite, and unweathered bedrock, and the CDF corrected for (Chemical erosion factor CEF; Riebe and Granger, 2013; Regard et al., 2016). Studies on catchment-wide denudation rates have not only been expanded from ¹⁰Be to in situ-produced ³⁶Cl in carbonates but also to incorporate the effect of deep weathering with dissolved solids (e.g., Ryb et al., 2014).

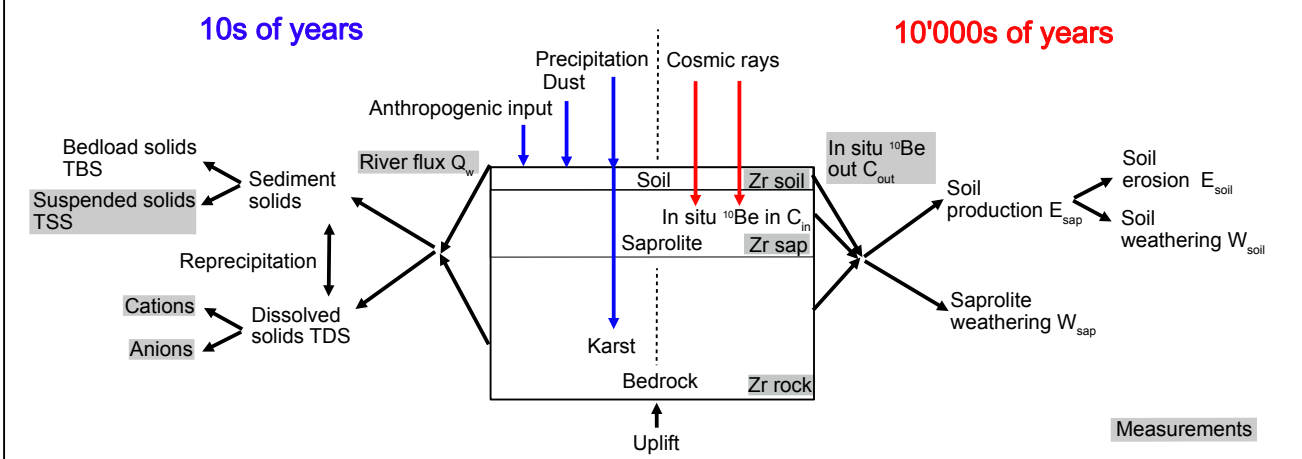
Furthermore, the coupling of in situ-produced ¹⁰Be in quartz and ³⁶Cl in carbonates from river sand allows the determination of both physical erosion and chemical weathering rates (e.g., Ott et al., 2022). In addition, physical erosion and chemical weathering rates of basaltic, silicate, and carbonate lithologies are more often determined with the technique of meteoric ¹⁰Be



65 (e.g., von Blanckenburg et al., 2012; Wittmann et al., 2015; Dannhaus et al., 2018; Wittmann et al., 2024). Such denudation rates have also been compared to rates derived from in situ-produced ^{10}Be in rivers draining silicate lithologies (e.g., VanLandingham et al., 2022).

One of the common challenges of methods that quantify surface change rates is understanding their spatial and temporal variability. The approach involving the comparison of rates based on river dissolved solids (over 10's of years) and in situ-produced cosmogenic nuclides (over 10 000's of years) encompasses different timescales (Figure 1). For instance, rates derived from in situ-produced cosmogenic ^{10}Be may integrate from the Last Glacial Maximum to the present, while rates based on river load span only the duration of time over which the measurements are recorded (e.g., 10s to ~100 years). In contrast, the method outlined by Riebe et al. (2004) reports both chemical weathering and physical erosion rates over thousands of years. However, this method may be limited by the spatial distribution of lithologies (e.g., Burke et al., 2007; Heimsath and Burke, 75 2013) and denudation hotspots (e.g., Larsen et al., 2014). Hence, each method and, more importantly, the combination of different methods, to quantify rates are subject to uncertainties specifically as most studies rely on integrating a number of measurements over diverse terrain.

A. Box model: River catchment



B. Equations: Total denudation $D = \text{physical erosion } E + \text{chemical weathering } W$

$$D = Q_w / A * (TSS + TBS + TDS) / \rho / 1000$$

$$TBS = TSS$$

$$TDS = \text{Cations} + \text{anions}$$

D	Total denudation rate
Q_w	River discharge
A	Catchment area
TSS	Total suspended solids
TBS	Total bedload solids
TDS	Total dissolved solids
Cations	$\text{Ca}^{2+}, \text{Mg}^{2+}, \text{Na}^+, \text{K}^+, \text{Si}^{4+},$
Anions	$\text{Cl}^-, \text{HCO}_3^-, \text{SO}_4^{2-}, \text{NO}_3^-$
ρ	Rock density

D	Total denudation rate	[mm/yr]
E	Rate of soil production or erosion	[mm/yr]
$W_{soil, sap}$	Rate of soil or saprolite weathering	[mm/yr]
$Zr_{soil, sap, rock}$	Immobile element concentration in soil, saprolite, rock	[ppm]
P_0	Nuclide production rate at surface	[atoms/(g*yr)]
C_{in}	Nuclide concentration produced in soil/saprolite	[atoms/g]
C_{out}	Average nuclide concentration in sediment	[atoms/g]
Λ	Attenuation length scale for production at depth	[g/cm ³]
ρ	Rock density	[g/cm ³]



80 **Figure 1: Approaches for the calculation of denudation rates.** Schematic overview of two different approaches to determine chemical weathering and physical erosion and, hence, total denudation rates for river catchments. The method based on river load gauging integrates over the last tens of years (left side). The method of in situ-produced denudation rate in combination with immobile elements integrates over tens of thousands of years (right side). (A) A box model indicating material fluxes and processes over these two timescales, and (B) the equations applied to these timescales, respectively.

In this study, decadal-scale physical erosion and chemical weathering rates derived from river load are investigated for
85 intermediate-sized river systems (71 to 12,710 km²) draining the Swabian Alb in Southwest Germany (Figure 2). These rates are compared to longer-term estimates of denudation from in situ-produced cosmogenic nuclides and geologic constraints on escarpment retreat and landscape evolution. The two rivers lie within a similar climate, but grade to different base-levels and contain different compositions of layered carbonate, evaporite, and siliciclastic lithologies in their individual sub-catchments
90 (Figure S1). This configuration allows addressing: (i) How do lithology and topography determine decadal-scale chemical weathering, physical erosion, and total denudation rates in the context of driving escarpment retreat? (ii) How do these decadal-scale rates compare to landscape evolution over longer timescales? (iii) How do the chemical depletion fractions CDFs of the Swabian Alb escarpment compare to global CDFs?

2 The Swabian Alb

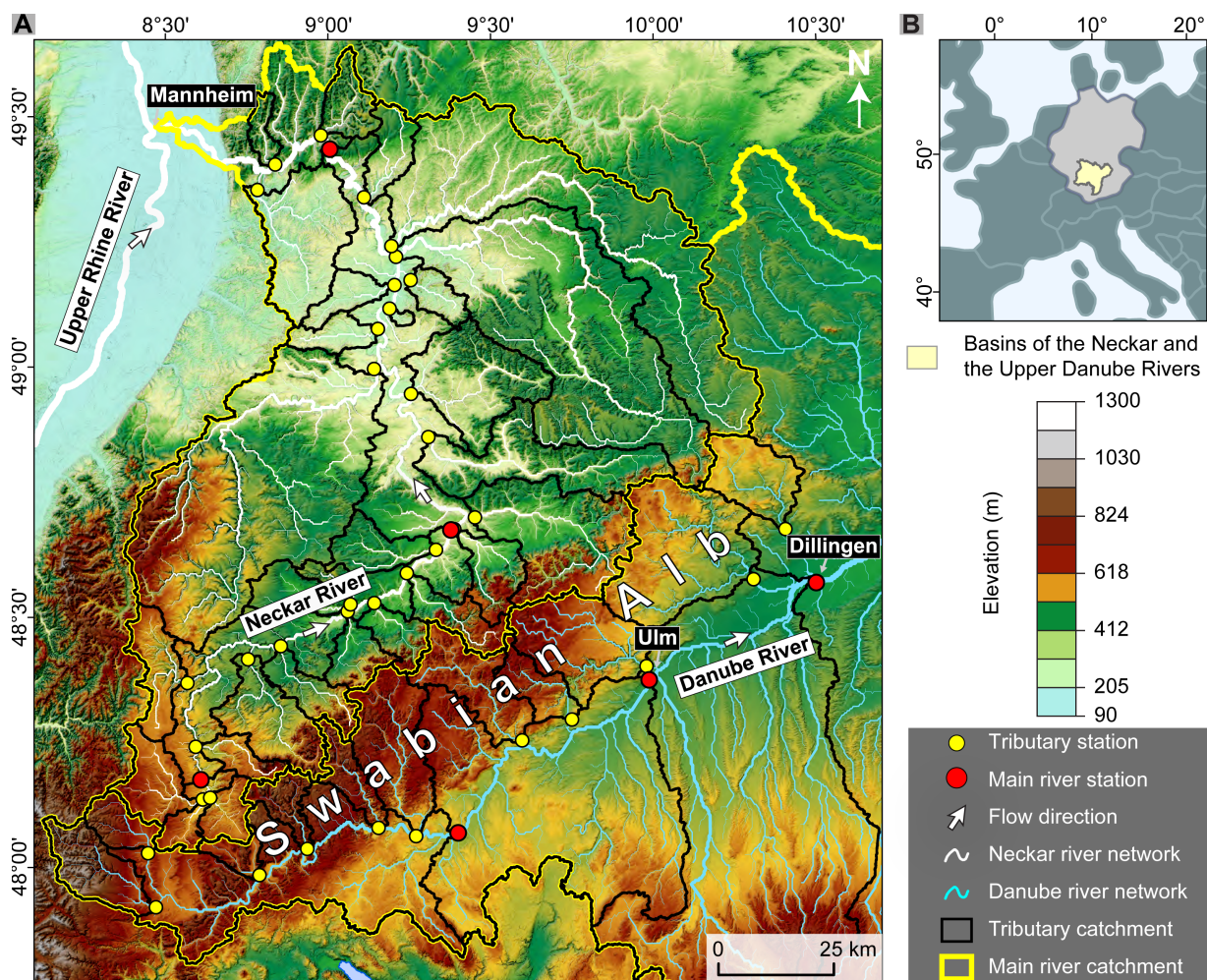
The Swabian Alb is a 200 to 400 m high escarpment in Southwest Germany, extending approximately 220 km from southwest
95 to northeast with a width ranging from 40 to 70 km (Figure 2). The escarpment is supported by Jurassic limestone bedrock units that gently dip to the Southeast (0 to 7 degrees), forming a tabular bench (tabular Jura). The Jurassic carbonates are the youngest unit within a 1 to 2-km thick package of alternating sandstone, evaporite, and carbonate stratigraphy (Littke et al., 2008). Triassic and early Jurassic deposits that underly the Swabian Alb escarpment encompass a variety of lithologies including siliciclastic formations (e.g., Buntsandstein, Keuper sandstone, Opalinus clay), carbonates (e.g., Muschelkalk;
100 Arietenkalk, Riffkalk), evaporites (e.g., Keuper gypsum), and are underlain by pre-Mesozoic crystalline basement rocks (Figure S1). The timing of uplift and subaerial exposure of the Swabian Alb is represented by an unconformity between the Jurassic carbonates and Cenozoic sedimentary cover of the Molasse basin and isolated deposits of Bohnerz (pisolithic iron oxides) in karst fissures with late-Eocene to Pleistocene mammal fossil assemblages. In the western most area of the Swabian Alb, paleosols of the Bohnerz formation indicate to be older than 5 Ma based on cosmogenic ³He concentrations (Hofmann et
105 al., 2017).

The Swabian Alb escarpment acts as a significant regional drainage divide (Figure 2). The divide separates rivers on the Swabian Alb that are incised into the Jurassic plateau and flow southeast into the Danube River, and rivers that start near the escarpment front and flow northwestward through the Jurassic and Triassic foreland towards the Neckar River (subsequently joining the Rhine River; Figure 2). These adjacent river systems exhibit contrasting base-level elevations, with the Neckar River's base-level in Mannheim lying at 83 m above sea level, while the Danube reaches 465 m in Ulm after a similar along-river distance. The regional divide is characterized by a pronounced cross-divide asymmetry, implying present-day systematic southward divide mobility (Winterberg and Willett, 2019). A combination of sediment provenance analysis and mapping of



fluvial features suggests that the Rhine River and its tributaries have expanded at the expense of the Danube River and its tributaries since the development of the Upper Rhine Graben (Davis, 1899; Petit et al., 1996; Villinger, 1998; Ziegler and Fraefel, 2009). This transition of formerly Danubian areas to the Rhine River and its tributaries, like the Neckar River, occurred through numerous discrete river capture events, several of which are well-documented (Villinger, 1998; Petit et al., 1996; Ziegler and Fraefel, 2009; Strasser et al., 2010; Yanites et al., 2013).

River load measurements have delivered decadal-scale physical erosion rates spanning from 0.004 to 0.011 mm/yr for both the Neckar River and Danube River (Blöthe and Hoffmann, 2022; Schaller et al., 2001; DGJ, 2006; DGJ, 2009). Reported chemical weathering rates in the Neckar River are estimated at approximately 0.020 mm/yr (Schaller et al., 2001), while total denudation rates range from 0.023 to 0.027 mm/yr (Schaller et al., 2001). Decadal-scale chemical weathering rates from small tributaries north of the Swabian Alb indicate lithology-specific chemical weathering rates (e.g., Hinderer, 2006). These rates range from 0.017 mm/yr for carbonate-rich Keuper sandstone, to 0.038 mm/yr for clay-dominated Middle Jurassic, and to rates exceeding 0.250 mm/yr for evaporites.





125 **Figure 2: Overview of the study area: Digital Elevation Modell (LGL-BW ATKIS Digitales Geländemodell DGM 5m, 2005) of the Swabian Alb escarpment area (Southwest Germany) with the two main drainage systems of Neckar River draining the Rhine River in the North and the Danube River to the Southeast. The points give locations of measurement stations providing data to calculate physical erosion and chemical weathering rates.**

The decadal-scale total denudation rates generally fall below the millennial-scale rates derived from cosmogenic nuclide analyses, which range between 0.055 and 0.135 mm/yr (Schaller et al., 2001 and 2002). This has been attributed to a possible under-representation of high-magnitude, low-frequency events in decadal-scale rates, the different integration timescale, or spatially non-uniform denudation in millennial-scale rates due to landslides along the escarpment during the Pleistocene (Terhorst, 2001). In addition, ¹⁰Be-derived denudation rates only reflect erosion of quartz-bearing lithologies, such as Triassic sandstones exposed in the foreland of the Swabian Alb. Long-term rock uplift rates are closer to existing denudation rate estimates from river loads. Periods of rock uplift above sea level are recorded by a regionally extensive early Miocene paleo-shoreline (cliff line) preserved along the southern edge of the Swabian Alb (0.05 mm/yr; Hofmann, 2017) and by locally preserved cave infills within the karstified limestone (0.01 mm/yr; Strasser et al., 2009). Cave infills on the Upper Jurassic contain abundant terrestrial fossils that are used to create a bio-stratigraphic record of karst evolution through time (Utrecht et al., 2016). Cave levels increase in age, moving to higher elevations within the Swabian Alb, and fossil assemblages shift to more brackish and marine environments in these oldest deposits, reflecting the progressive lowering of regional baselevel during the late Cenozoic (Abel et al., 2002; Utrecht et al., 2016).

3 Methods

In order to evaluate denudation rates for the Swabian Alb-draining rivers, lithologies and catchment-averaged metrics are extracted. Comparing different approaches, decadal-scale chemical weathering and physical erosion rates are calculated from 145 river discharge and river load, and then transformed into Swabian Alb escarpment retreat rates, where applicable.

3.1 Lithologies and catchment-average metrics

These metrics encompassed catchment area, mean elevation, local relief, hillslope angle, local channel slope normalized by upstream drainage area, mean annual precipitation, mean annual temperature, vegetation cover, and lithological composition (Table S1 and S2). We utilized a 5 m digital elevation model (DEM) sourced from Baden-Württemberg's State Institute for the Environment (LGL-BW ATKIS Digitales Geländemodell DGM 5m, 2005) to extract catchment metrics widely used to unravel patterns and rates of physical erosion and chemical weathering across diverse landscapes (e.g., Ahnert, 1970; Montgomery and Brandon, 2002; DiBiase et al., 2010; Portenga and Bierman, 2011; Harel et al., 2016). Catchments were extracted from the DEM with the TopoToolbox software (Schwanghart and Scherler, 2014), employing existing measurement stations (discharge, solute solids, and dissolved solids) as pour points. Local relief was determined as the elevation range within 150 a 1.5-kilometer diameter circular neighborhood (e.g., DiBiase et al., 2010; Peifer et al., 2021). Hillslope angle was computed from fitting a 3-by-3 cell plane for each DEM cell using the Least Squares Method. A comparison of local channel slope



normalized by upstream drainage area and a regional reference concavity was calculated using the empirical power-law relationship between local channel slope (S) and upstream drainage area (A) (Eq. (1); Flint, 1974):

$$S = k_{sn} A^{-\theta_{ref}} \quad (1)$$

160 A reference channel concavity (θ_{ref}) of 0.45 was used to compare a normalized fluvial relief (k_{sn}) across stream segments or watersheds with different drainage areas (Kirby and Whipple, 2012). The river network was extracted using an upslope area threshold for channel initiation of 1 km^2 and a smoothing window of 100 m was used to calculate local channel slope, S . We computed catchment-averaged k_{sn} to compare fluvial relief between basins with suspended sediment and solute load data (Forte and Whipple, 2019).

165 Catchment-averaged mean annual precipitation rates and mean annual temperature were extracted from the CHELSA (Climatologies at high resolution for the Earth's land surface areas) version 2 climatology dataset covering the years 1981 to 2010 (Karger et al., 2017; Karger et al., 2021). This dataset provides high-resolution (30 arcsec) estimates of precipitation and temperature derived from downscaled ERA-Interim climatic reanalysis. Vegetation cover was estimated using Copernicus Land Monitoring Service's (CLMS) long-term statistics of NDVI (Normalized Difference Vegetation Index) over the period 170 between 1999-2019 (European Commission Directorate-General Joint Research Centre, 2021; Léon-Tavares et al., 2021). NDVI, defined as $NDVI = (NIR - Red)/(NIR + Red)$, relies on reflectance measurements in the near-infrared (NIR) and red (Red) bands.

Lithological data were extracted from the 'General Geological Map of the Federal Republic of Germany' dataset, mapped at a scale of 1:250,000 (BGR, 2019). The extracted lithologies are bundled into 10 bins (Table S2), which are then further classified 175 into three categories, including carbonates (Upper Jura), carbonates with evaporites and siliciclastic lithologies (Middle Triassic), and combined silicate and siliciclastic lithologies (Proterozoic, Paleozoic; Lower and Upper Triassic, Lower and Middle Jurassic, Tertiary and Quaternary). The attribution of Upper Triassic, Lower and Middle Jurassic to the siliciclastic bin is questionable as oxidation of Fe-sulfides in clay and mudstone may contribute SO_4^{2-} , which is only attributed to weathering of evaporites in this study.

180 **3.2 Decadal-scale rates from river load**

Decadal-scale rates from river load are investigated for tributaries to the Neckar River from its source to its confluence into the Rhine River, and for the Danube River and its southward draining tributaries of the Swabian Alb (Danube Swabian Alb tributary) from its source to Dillingen, the downstream most gauge site of the Danube River still draining the Swabian Alb (Figure 2). Neckar tributaries were separated into tributaries having a drainage divide with Danube tributaries on the Swabian 185 Alb (called Neckar Swabian Alb tributary) and all remaining Neckar tributaries in the Swabian Alb foreland (Neckar foreland tributary).



Drainage area (A), river discharge (Q), and total suspended and dissolved solids of a river (TSS and TDS , respectively) are used to calculate decadal-scale physical erosion (E) and chemical weathering rates (W ; Figure 1, left side). In the context of this study, all data is extracted from online available state databases (e.g., LUBW 2023; GKD, 2023). The different data sets 190 do not integrate over the same timescales nor is the collected sample material analyzed in the exact same way. Hence, the calculated rates need to be considered cautiously. Data on river discharge (Table S3; daily mean values over ~30 to 60 years) for the Neckar River (3 stations; DGJ, 2009) and some of its tributaries (26 stations; DGJ, 2009; LUBW, 2023) alongside the Danube River (3 stations; DGJ, 2006) and some of its tributaries are consolidated (11 stations; DGJ, 2006; LUBW 2023). Weathering rates are based on dissolved solids (single measurement every month for ~10 years) extracted from 29 stations for 195 the Neckar River and tributaries (LUBW, 2023) and 12 for the Danube River and its Swabian Alb tributaries (LUBW, 2023; GKD, 2023). Suspended solids measurements are less abundant (single measurement every two months for ~20 to 40 years) and are combined with discharge to calculate physical erosion rates.

The calculation of chemical weathering rates relied on using dissolved solids generally comprised of the total concentration of major cations (Ca^{2+} , Mg^{2+} , Na^+ , K^+ and Si^{4+}) along with Cl^- , SO_4^{2-} , and HCO_3^- (Table S4). Si^{4+} values were unavailable and 200 HCO_3^- concentrations were derived from reported pH and alkalinity. To calculate chemical weathering rates, concentrations can be corrected for atmospheric and anthropogenic inputs, as well as for secondary calcite precipitation. This study presents three different approaches to calculate chemical weathering rates (Table 1; Table S5): CWR 1) Uncorrected rate; CWR 2) Correction for rain input (Agster, 1986) and attribution of all Cl^- to road salt; and CWR 3) Combining CWR 2 with the assumption that 90% of the originally dissolved Ca^{2+} concentration has reprecipitated (e.g., Erlanger et al., 2021). The 205 uncorrected CWR 1 attributes the SO_4^{2-} concentration to be entirely the weathering product of gypsum/anhydrite and not to the oxidation of Fe-sulfides in clay (e.g., Opalinus clay; Hinderer 2006). CWR 2 corrects for rain input, assuming that half of the catchment area is cultivated and the other half is forested. This assumption influences the correction of the chemical weathering rate for rain input CWR 2 only marginally, as rain input contributes generally less than 5% to the total dissolved load. CWR 2 is reporting a minimum rate as NaCl attributed to road salt could also be released by rock salt, which is present 210 in the middle Triassic Muschelkalk formation. In contrast, CWR 3 is considered a maximum rate, as a 90% fraction of Ca reprecipitation of Ca is likely a maximum estimate (Erlanger et al., 2021) and some Ca is weathered from gypsum in the Muschelkalk and lower Keuper formations. In addition, to make these corrections for chemical weathering rates, the different contributions of carbonate, silicate/siliciclastic, and evaporite weathering are estimated following the approach presented in Campbell et al. (2022).

215 Three different physical erosion rates PER are calculated using the available suspended solids (Table S6), catchment area, river discharge (Table S3), and a sediment density of 2.7 g/cm^3 (Table 1). Whereas PER 1 is based on average suspended solids and average discharge, PER 2 is estimated from abundant discharge values using the empirical relation between individual discharge and suspended solids. A maximum rate PER 3 results from further correction of PER 2 for an addition of



bedload. This correction assumes a bedload to total sediment flux ratio of 0.5 from the compilation of Turowski et al., (2010)
220 for sand-bedded rivers.

Three total denudation rates TDR, which encompass both physical erosion and chemical weathering rates, are documented for the measurement stations (Table 1). TDR 1 is the sum of PER 1 and CWR 1, representing an uncorrected total denudation rate. TDR 2 is a corrected total denudation rate based on PER 3 (corrected for bedload) and CWR 2 (corrected for rain and road salt input). TDR 3 is the sum of PER 3 and CWR 3, suggesting a maximum total denudation rate.

225 Based on these different rates, three chemical depletion fractions CDF (e.g., Riebe et al., 2004), are calculated by dividing the chemical weathering rate by the total denudation rate (Table 1). Whereas CDF 1(CWR 1 over TDR 1) results in maximum values for CDFs, CDF 2 (CWR 2 over TDR 2) represents minimum values. Values of CDF 3 (CWR 3 divided by TDR 3) report values between CDF 1 and CDF 2. In addition, the corrected physical erosion PER 3, the chemical weathering CWR 2 corrected for rain and anthropogenic input, and the total denudation Rate TDR 2 are analyzed for correlations with geomorphic,
230 climatic/biotic, and lithologic parameters (see Chapter 3.2). The four reported correlation sets include all tributary data of the Neckar and Danube Rivers.

The vertical denudation rates are transformed into horizontal retreat rates for the Swabian Alb escarpment with approaches presented by Wang and Willett (2021). However, instead of calculating a denudation rate from cosmogenic nuclides in river sand, the total denudation rates from river load (TDR 2) are directly converted into retreat rates. Two different retreat rates are
235 presented: 1) Basin projection method (RR 1); and 2) Basin projection method (RR 2), considering reduced denudation of the plateau area (Wang et al., 2021). The transformation of the vertical denudation rate into a horizontal rate is performed for one retreat direction, which is perpendicular to the mean orientation of the shared drainage divide between two adjacent and competing catchments. For RR 2, the denudation rate of the plateau area is given by the total denudation rate TDR 2 of Danube Swabian Alb tributaries sharing catchment divides with the Neckar Swabian Alb tributaries (Table 2).

240 4 Results

4.1 Decadal-scale rates from river load

Uncorrected chemical weathering rates (CWR 1) from the Neckar River and its tributaries are highly variable and range over two orders of magnitude, from 0.005 to 0.096 mm/yr (Figure 3A; Table 1). Tributaries draining the escarpment of the Swabian Alb show generally higher chemical weathering rates than the Neckar foreland tributaries that drain older Mesozoic bedrock units. CWR1 for the Danube River and its Swabian Alb tributaries are more homogenous and below 0.050 mm/yr (Figure 3B).
245 These observations made for CWR 1 are the same for CWR 2 corrected for rain and anthropogenic input (Figure 4A). The average weathering rate for the Neckar Swabian Alb tributaries (0.054 mm/yr) is double the average rate for the Danube Swabian Alb tributaries (0.026 mm/yr). Similar trends are also visible for CWR 3 corrected for secondary calcite precipitation



just with values as high as 0.300 mm/yr for Swabian Alb tributaries of the Neckar River and 0.150 mm/yr for Swabian Alb 250 tributaries of the Danube River (Table 1). Whereas CWR 3 is considered a maximum rate, CWR 2 represents a minimum rate.

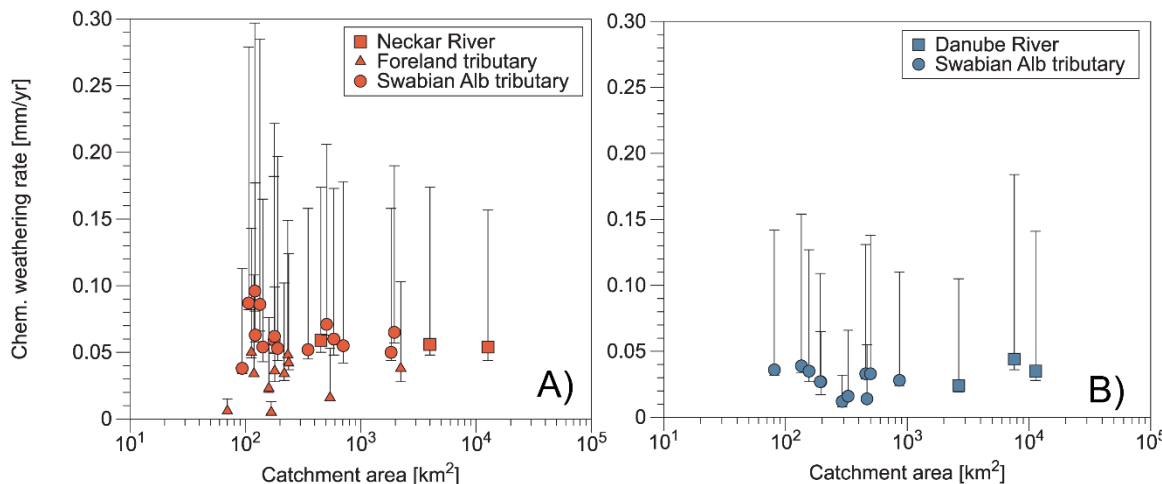


Figure 3: Decadal-scale chemical weathering rates versus catchment area: Uncorrected chemical weathering rates (CWR 1) from river dissolved solids versus catchment area for: A) the Neckar River (Red squares), its foreland tributaries (Red triangle), and its Swabian Alb tributaries (Red circles) and B) the uppermost reach of the Danube River (Blue squares) and its Swabian Alb tributaries (Blue circles). Error bars comprise the difference between CWR 1 and the rate corrected for rain and road salt input (CWR 2, a minimum scenario) and the rate considering secondary calcite precipitation (CWR 3, a maximum scenario).

255

260

Physical erosion PER 1 based on the average suspended solids and discharge of rivers ranges from below 0.001 to 0.002 mm/yr for all analyzed rivers (Table 1). In contrast, PER 2 can be as high as 0.036 mm/yr for Neckar tributaries but is still low for the Danube River and its Swabian Alb tributaries (0.000 to 0.002 mm/yr; Table 1). Correction for bedload increases the physical erosion PER 3 in tributaries of the Neckar River to 0.072 mm/yr, whereas the Danube River and its Swabian Alb tributaries stay below 0.005 and 0.004 mm/yr, respectively (Figure 4B). The resulting total denudation TDR 1 ranges from 0.005 to 0.098 mm/yr, TDR 2 from 0.005 to 0.137 mm/yr (Figure 4C), and TDR 3 may be as high as 0.336 mm/yr (Table 1). The main general trend is that the rates of Neckar tributaries are more heterogeneous and higher than values from the Danube and its Swabian Alb tributaries (Figure 4C).

265

270

275

Table 1: Compilation of chemical weathering, physical erosion, and total denudation rates for the Swabian Alb escarpment. (#) Rivers in grey italics are left-side tributaries of the Neckar River. (1) Uncorrected chemical weathering rate based on dissolved load. (2) Chemical weathering rate corrected for input by rain and road salt. (3) Chemical weathering rate corrected for rain, road salt, and secondary Ca precipitation of 90%. (4) Uncorrected physical erosion rate based on average discharge and solute load. (5) Physical erosion rate based on power law function through discharge and solute load. (6) Physical erosion rate 2 multiplied by 2 assuming that bedload over solute load is 1.0. (7) Total denudation rate based on physical erosion rate 1 and chemical weathering rate 1. (8) Total denudation rate based on physical erosion rate 3 and chemical weathering rate 2. (9) Total denudation rate based on physical erosion rate 3 and chemical weathering rate 3. (10) CDF based on chemical weathering rate 1 over total denudation rate 1. (11) CDF based on chemical weathering rate 2 over total denudation rate 2. (12) CDF based on chemical weathering rate 3 over total denudation rate 3.



River	Area km ²	Chemical weathering			Physical erosion			Total denudation			CDF 1 ⁽¹⁰⁾	CDF 2 ⁽¹¹⁾	CDF 3 ⁽¹²⁾
		CWR 1 ⁽¹⁾	CWR 2 ⁽²⁾	CWR 3 ⁽³⁾	PER 1 ⁽⁴⁾	PER 2 ⁽⁵⁾	PER 3 ⁽⁶⁾	TDR 1 ⁽⁷⁾	TDR 2 ⁽⁸⁾	TDR 3 ⁽⁹⁾			
	mm/yr												
Neckar	453	0.059	0.050	0.165	0.001	0.005	0.009	0.060	0.059	0.174	0.98	0.85	0.95
Neckar	3337	0.056	0.048	0.166		0.005	0.010		0.058	0.176		0.82	0.94
Neckar	12710	0.053	0.043	0.147									
Mean Neckar		0.056	0.047	0.159	0.001	0.005	0.007	0.010	0.060	0.058	0.175	0.98	0.84
<i>Eschach</i>	218	0.034	0.029	0.097	0.000	0.000							
Prim	121	0.096	0.081	0.283	0.001	0.004	0.001	0.034	0.030	0.098	0.99	0.97	0.99
Schlüchtern	107	0.087	0.082	0.274		0.008		0.098	0.089	0.291	0.99	0.91	0.97
<i>Glatt</i>	234	0.048	0.042	0.143	0.001	0.002							
Eyach	350	0.052	0.044	0.150	0.001	0.021	0.003	0.049	0.045	0.146	0.98	0.92	0.98
Starzel	178	0.059	0.050	0.173	0.002	0.015	0.043	0.053	0.087	0.193	0.98	0.51	0.78
Steinlach	142	0.054	0.043	0.154	0.000	0.001	0.030	0.061	0.080	0.203	0.97	0.63	0.85
<i>Ammer</i>	238	0.042	0.037	0.119	0.000	0.001	0.003	0.054	0.045	0.156	0.99	0.94	0.98
Echaz	134	0.086	0.065	0.265	0.001	0.036	0.001	0.042	0.038	0.120	0.99	0.97	0.99
Erms	179	0.062	0.049	0.210	0.001	0.003	0.072	0.087	0.137	0.336	0.99	0.48	0.79
<i>Aich</i>	180	0.036	0.027	0.090	0.001	0.005	0.004	0.063	0.053	0.213	0.98	0.93	0.98
Lauter	191	0.053	0.044	0.188	0.001	0.002	0.010	0.036	0.037	0.100	0.98	0.73	0.90
Fils	707	0.055	0.042	0.165	0.001	0.007	0.004	0.054	0.048	0.192	0.98	0.93	0.98
Rems	586	0.060	0.048	0.160	0.002	0.005	0.015	0.057	0.057	0.180	0.97	0.74	0.92
Murr	507	0.071	0.063	0.198	0.002	0.006	0.010	0.062	0.058	0.171	0.97	0.82	0.94
<i>Enz</i>	2228	0.038	0.029	0.094	0.002	0.011	0.012	0.073	0.075	0.210	0.97	0.84	0.94
Zaber	113	0.050	0.046	0.140	0.000	0.000	0.022	0.040	0.051	0.116	0.96	0.57	0.81
Schozach	94	0.038	0.034	0.109		0.000		0.051	0.046	0.140	0.99	0.99	1.00
<i>Lein</i>	119	0.034	0.032	0.106									
Sulm	122	0.063	0.058	0.172									
Kocher	1960	0.065	0.057	0.181	0.002	0.008							
Jagst	1838	0.050	0.044	0.153	0.002	0.002	0.016	0.067	0.073	0.197	0.96	0.78	0.92
Elz	160	0.023	0.020	0.072		0.005		0.052	0.049	0.158	0.96	0.90	0.97
Itter	168	0.005	0.004	0.012	0.000	0.001							
Steinach	70	0.006	0.004	0.013		0.001		0.005	0.005	0.013	0.94	0.75	0.90
<i>Elsenz</i>	543	0.016	0.014	0.050	0.000	0.001							
Mean Neckar trib.		0.049	0.042	0.145	0.001	0.007	0.010	0.002	0.016	0.053		0.85	
Mean Swabian trib.		0.066	0.055	0.198	0.001	0.010	0.015	0.013	0.055	0.056	0.164	0.98	0.81
Danube	2647	0.030	0.025	0.106	0.001	0.002	0.004	0.031	0.028	0.110	0.97	0.87	0.97
Danube	7588	0.054	0.046	0.186									
Danube	11350	0.044	0.036	0.142									
Mean Danube		0.042	0.036	0.145	0.001	0.002	0.004	0.031	0.028	0.110	0.97	0.87	0.97
Breg	292	0.012	0.009	0.028	0.001	0.002	0.003	0.013	0.012	0.031	0.94	0.74	0.90
Brigach	195	0.027	0.016	0.055	0.001	0.001	0.002	0.028	0.019	0.057	0.97	0.87	0.96
Elta	81	0.036	0.032	0.138	0.001	0.001	0.001	0.037	0.033	0.139	0.98	0.97	0.99
Bära	135	0.039	0.034	0.149	0.000	0.001	0.002	0.039	0.036	0.151	1.00	0.94	0.99



Schmeie	156	0.035	0.027	0.119	0.001	0.001	0.002	0.036	0.029	0.121	0.99	0.94	0.98
Lauchert	456	0.033	0.029	0.127	0.001	0.001	0.002	0.034	0.031	0.129	0.98	0.94	0.98
Grosse Lauter	327	0.016	0.014	0.064	0.001	0.001	0.001	0.016	0.016	0.065	0.96	0.91	0.98
Schmiech	193	0.027	0.025	0.107	0.001	0.000	0.001	0.027	0.026	0.108	0.98	0.96	0.99
Blau	499	0.033	0.030	0.134									
Brenz	864	0.028	0.024	0.106	0.002	0.000	0.001	0.030	0.025	0.107	0.93	0.96	0.99
Egau	467	0.014	0.013	0.054									
Mean Danube trib.		0.027	0.023	0.098	0.001	0.001	0.002	0.029	0.025	0.101	0.97	0.92	0.97

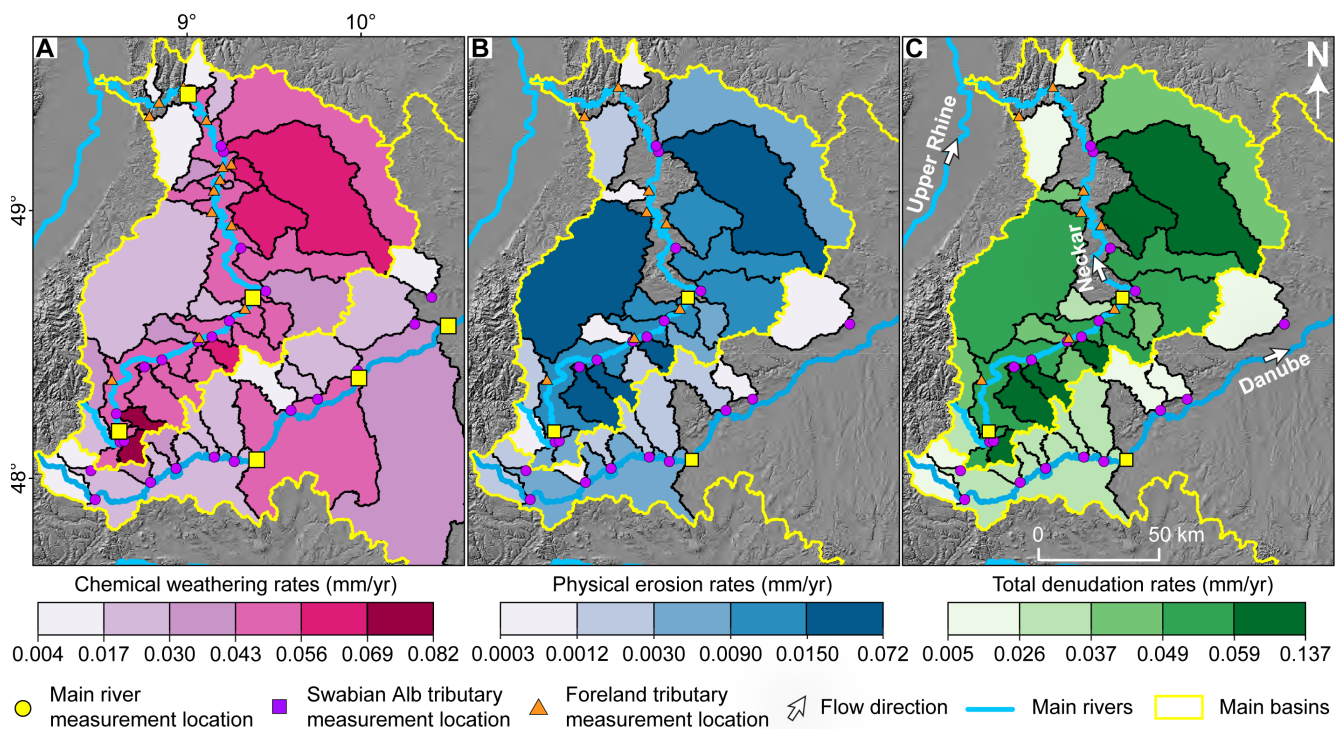


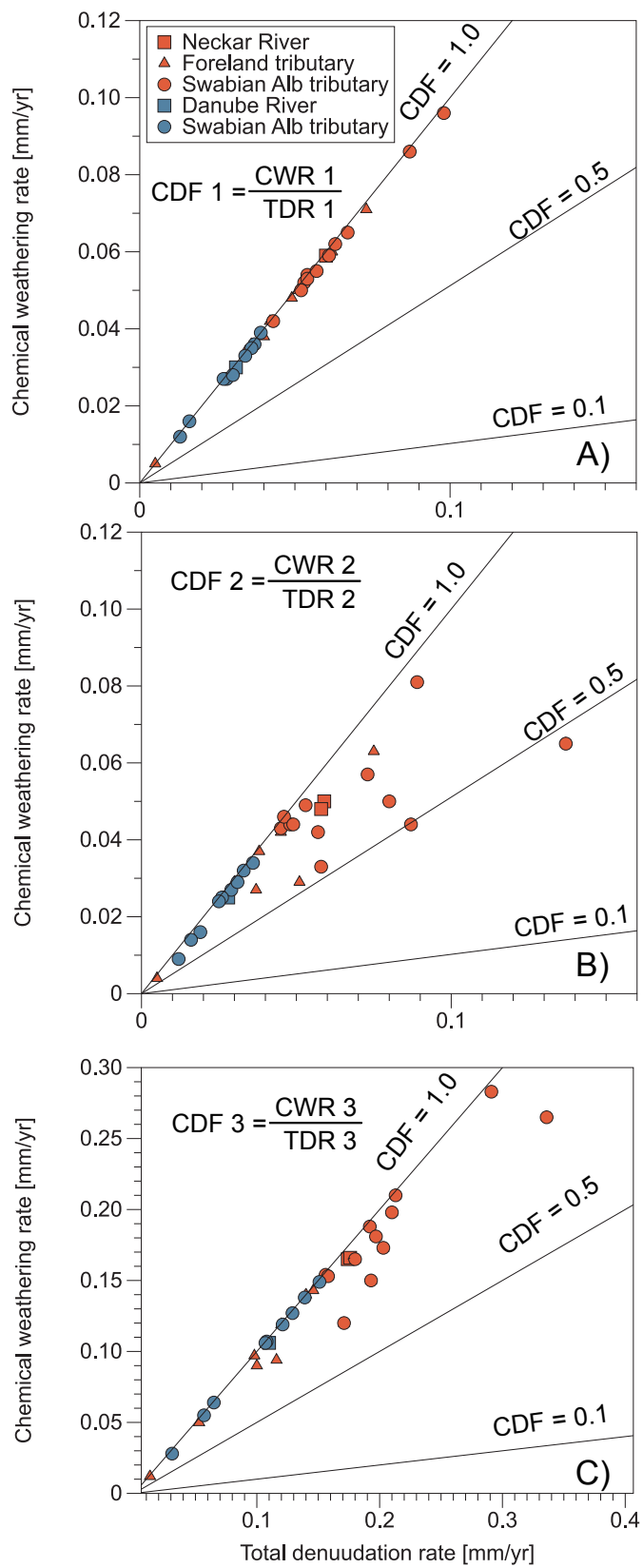
Figure 4: Mean spatial decadal-scale denudation rates: Maps (LGL-BW ATKIS Digitales Geländemodell DGM 5m, 2005) showing calculated rates in catchments of the Neckar River and Upper Danube River and their tributaries, respectively. A) Minimum chemical weathering rate CWR 2 derived from dissolved solids. B) Maximum physical erosion rates PER 3 from suspended load and bedload. C) Total denudation rates TDR 2 as the sum of physical erosion PER 3 and chemical weathering rates CWR 2.

280

285

Comparing the fraction of chemical weathering on total denudation, CDF 1 (calculated with the raw data) shows little variability (values between 0.94 and 1.00). CDF 2, based on corrections of rain and road salt, yields the strongest spread in values, and CDF 3 shows some outliers for the Neckar tributaries (Figure 5). Generally, CDF values range from 0.48 to almost 1.00 for the Neckar tributaries and from 0.74 to 0.99 for Danube Swabian Alb tributaries.

Escarpment retreat rates RR 1 based on basin projection and TDR 2 range from 1.2 to 9.3 mm (Average: 3.9 mm/yr). Rates (RR 2), which consider lower denudation rates of plateau areas, are only slightly lower (Average: 3.5 mm/yr).





290 **Figure 5: Effect of correcting the decadal-scale chemical weathering rates: Chemical weathering rate versus total denudation rate**
295 for the Neckar River and its Swabian Alb tributaries as well as for the Danube River and its Swabian Alb tributaries. A) Uncorrected
rates (Chemical weathering rate CWR 1 and physical erosion rate PER 1). B) Correction of chemical weathering rates for rain and
296 road salt input (CWR 2) and physical erosion rate for power law function and river bedload (PER 3). C) Correction of chemical
weathering rate for secondary calcite precipitation (CWR 3) and physical erosion rate for power law function and river bedload
(PER 3).

300 **Table 2: Escarpment retreat rates of the Swabian Alb based on Wang and Willett (2021) and Wang et al. (2021). (1) Total denudation
rate TDR 2 based on chemical weathering rate CWR 2 and physical erosion rate PER 3. (2) Retreat rate based on basin projection
method and total denudation rate TDR 2. (3) Retreat rate based on basin projection method corrected for low denudation TDR 2 of
plateau area.**

River	TDR 2 ⁽¹⁾ mm/yr	River	TDR 2 ⁽¹⁾ mm/yr	Retreat Direction °	Retreat Rate 1 Basin projection ⁽²⁾ mm/yr	Retreat Rate 2 Basin projection ⁽³⁾ mm/yr
Neckar tributaries						
Prim	0.089	Elta	0.033	135.0	2.7	2.7
Schlachem		Bära	0.036	135.0		
Eyach	0.087	Schmeie	0.029	135.0	4.2	4.2
Starzel	0.080	Lauchert	0.031	135.0	3.4	2.9
Steinlach	0.045	Lauchert	0.031	157.5	1.2	1.2
Echaz	0.137	Grosse Lauter	0.016	135.0	4.2	4.0
Erms	0.053	Schmiech	0.026	135.0	2.0	1.6
Lauter	0.048	Schmiech	0.026	180.0	1.7	1.4
Fils	0.057	Brenz	0.025	157.5	3.8	3.7
Rems	0.058	Brenz	0.025	157.5	3.8	3.7
Kocher	0.073	Brenz	0.025	180.0	9.3	9.2
Jagst	0.049			180.0	6.8	
Mean	0.071		0.027	151.9	3.9	3.5

4.2 Correlation of catchment metrics with denudation rates

305 Statistically significant correlations with rates (CWR 2, PER 3, and TDR2) for all investigated catchments are reported for
only a few metrics (Table 3; Table S7; Figure S2 to S4). The corresponding P values for all correlations reported here is P
<0.05. CWR 2 correlates with mean annual precipitation ($R = -0.38$) and some lithologies but no topographic metrics. Whereas
the abundance of the Lower Triassic (e.g., sandstone) correlates negatively, Upper Triassic (e.g., sandstone and marl), Lower
Jurassic (e.g., claystone), and Middle Jurassic (e.g., claystone) correlate positively with CWR 2. PER 3 show positive
correlations with maximum relief ($R = 0.44$), Lower Jurassic ($R = 0.46$), and Middle Jurassic ($R = 0.36$). TDR 2 indicate
positive correlations with maximum relief ($R = 0.44$) and a negative correlation with mean annual precipitation ($R = -0.39$).
310 TDR 2 correlates negatively with Lower Triassic (e.g., sandstone) and positively with Lower and Middle Jurassic (e.g.,
claystone).

CWR 2 of the Neckar Swabian Alb tributaries (Table S8) correlate positively with mean elevation ($R = 0.57$) and strongly
negative with maximum relief ($R = -0.84$). CWR 2 also correlates negatively with mean annual temperature. In addition, CWR
2 correlates positively with the percentage of the lithology for the Lower Jurassic (e.g., claystone). No significant correlations



315 were found for PER 3 and TDR 2. In the case of the Danube Swabian Alb tributaries (Table S9), positive correlations of PER 3 and mean elevation ($R = 0.85$), maximum relief ($R = 0.71$), and mean annual precipitation ($R = 0.82$) were reported. PER 3 correlates negatively with mean annual temperature ($R = -0.91$). A negative correlation of TDR 2 with mean annual precipitation was observed ($R = -0.67$).

Table 3: Correlations between rates and mean catchment metrics, given for all data, Neckar Swabian Alb tributaries.

	All data			Neckar Swabian tributaries			Danube Swabian tributaries		
	CWR <i>n</i> =43	PER <i>n</i> =32	TDR <i>n</i> =32	CWR <i>n</i> =12	PER <i>n</i> =11	TDR <i>n</i> =11	CWR <i>n</i> =11	PER <i>n</i> =9	TDR <i>n</i> =9
Catchment area	0.06	0.05	0.06	-0.24	-0.22	-0.24	-0.03	-0.25	-0.16
Mean elevation	-0.09	-0.14	-0.23	0.57	0.15	0.30	0.02	0.86	-0.10
Max. relief	0.14	0.44	0.44	-0.84	0.08	-0.31	0.00	0.71	-0.34
Local relief (1000m)	-0.02	0.23	0.15	-0.12	0.24	0.14	0.34	0.35	0.38
Mean ksn	-0.13	0.20	0.05	-0.24	0.13	-0.01	0.17	0.53	0.10
Slope	-0.02	0.21	0.14	-0.13	0.25	0.15	0.27	0.46	0.27
MAP	-0.38	-0.25	-0.39	-0.16	-0.43	-0.53	-0.57	0.82	-0.67
MAT	0.14	0.16	0.26	-0.60	-0.12	-0.28	0.06	-0.91	0.19
Vegetation cover	-0.07	0.00	-0.05	0.13	-0.17	-0.13	-0.52	0.56	-0.43
Lower Triassic	-0.47	-0.11	-0.34						
Middle Triassic	0.03	-0.11	-0.06	-0.09	-0.12	-0.16			
Upper Triassic	0.40	0.11	0.31	0.09	-0.11	-0.02			
Lower Jurassic	0.66	0.46	0.64	0.70	0.18	0.39			
Middle Jurassic	0.50	0.35	0.49	0.15	0.13	0.15	0.41	-0.34	0.44
Upper Jurassic	-0.21	-0.13	-0.21	-0.28	0.04	-0.06	0.41	-0.47	0.43
Tertiary	-0.24	-0.16	-0.23				-0.16	-0.61	-0.01
Quaternary	0.11	0.09	0.14	-0.51	0.00	-0.14	0.58	-0.25	0.57

$p > 0.05$

$R^2 0 \text{ to } 0.3, p < 0.05$



$R^2 0.3 \text{ to } 0.5, p < 0.05$



$R^2 0.5 \text{ to } 0.7, p < 0.05$



$R^2 0.7 \text{ to } 1.0, p < 0.05$



320

5 Discussion

The discussion is organized into three sections exploring (i) the decadal-scale chemical weathering, physical erosion, and total denudation rates across all datasets, with a particular emphasis on tributaries of the Neckar River and Danube River within the Swabian Alb, (ii) evaluating the total denudation rates observed in the Swabian Alb with rates documented in other studies 325 spanning various longer timescales, and (iii) discussing the contribution of chemical weathering and physical erosion to total denudation rates, leveraging global datasets and employing diverse methodologies to ascertain rates.



5.1 Decadal-scale rates versus catchment metrics

5.1.1 Interpretation of measured rates

In the following section, the different rates reported in this study are compared to other decadal-scale rates in the study area.

330 The uncorrected (CWR 1) and rain/salt-corrected (CWR 2) decadal-scale chemical weathering rates from all Neckar tributaries (Figure 3A and 4A; average 0.042 mm/yr) agree well with decadal-scale rates reported from small catchments in the Swabian Alb foreland and the Swabian Alb itself (Hinderer, 2006). These rates ranged from 0.017 mm/yr for carbonate-rich sandstone over 0.038 mm/yr for carbonate-rich claystone to values of > 0.250 mm/yr for evaporites. The average of chemical weathering rates from these small catchments are comparable to CWR 2 for larger catchments, which contain a mix of each of these 335 lithologies. In contrast, the corrected rates CWR 2 for the Neckar River are twice as high as the corrected weathering rates of Schaller et al. (2001), which may result from different data sets (e.g., time span and frequency of measurements). Furthermore, the incorporation of a correction for secondary calcite precipitation (CWR 3) introduces additional differences in chemical weathering rates. The physical erosion rates (PER 3; Figure 4B) for the Neckar River are comparable to published rates of ~0.010 mm/yr (Blöthe and Hoffmann, 2022; DGJ, 2006) and ~0.005 mm/yr (Schaller et al., 2001). In contrast, the physical 340 erosion rates PER 3 for the Danube River and its Swabian Alb tributaries are smaller than the already relatively low value of 0.005 mm/yr for the Danube River (DGJ, 2006; Figure 4B). The maximum physical erosion rates (PER 3) assume that sediment load measurements capture a representative distribution of discharges during the measurement period, but likely under sample infrequent high-magnitude events that contribute high suspended and bedload sediment fluxes relative to solute loads (Pratt-Sitaula et al., 2007; Turowski et al., 2010). Nevertheless, a relative comparison shows that physical erosion rates in the Neckar 345 Swabian Alb tributaries are at least two times higher than rates from Danube Swabian Alb tributaries (Figure 4B). Hence, the total denudation rates (TDR 2), which correspond to a composite of chemical weathering and physical erosion rates, are at least two times higher in the Neckar Swabian Alb tributaries than the Danube Swabian Alb tributaries as well as Swabian Alb foreland tributaries (Figure 4C). Overall, the reported rates CWR 1 to 3 and PER 2 to 3 from the Neckar Swabian Alb tributaries 350 are generally twice as high as the CWRs of the Danube Swabian Alb tributaries (Figure 3 and 4A); however, maximum physical erosion rate estimates could be underestimated in both records. Finally, it is worth noting (Fig. 4) that despite the similar tectonic, climate and biological settings considered in this study, the inter-catchment variations in chemical weathering, physical erosion, and total denudation rate can vary by a factor of 10 across drainage divides for rivers sharing a common main river (Neckar, or Danube). This result is explored in the next section, but could largely be due to lithologic variations between catchments.

355 **5.1.2 Interpreted driver of rates**

We interpret differences in chemical weathering, physical erosion, and total denudation rates between the Neckar Swabian Alb tributaries and Danube Swabian Alb tributaries to reflect the contrast in baselevel, which has been set by the organization of major river systems since the evolution of the Upper Rhine Graben and onset of long-wavelength uplift in Middle Miocene



times (e.g. Ring and Bolhar, 2020). We reason that the contrast in baselevel can affect chemical, physical, and total denudation rates in two ways. Lower baselevel on the Neckar side of the escarpment (1) increases topographic relief to drive physical erosion and chemical weathering of the subsurface and (2) exposes layered stratigraphy with a range of susceptibilities to physical erosion and chemical weathering. The climate is comparable on the two sides of the Swabian Alb and the nearly flat-lying Mesozoic strata indicate that differential uplift is minor across the spatial scales of the catchments analyzed, so we focus our discussion on differences in lithology and relief across the escarpment and their controls on physical erosion and chemical weathering.

The steep north-facing escarpment is drained by the Neckar Swabian Alb tributaries eroding the Upper Jurassic caprock and underlying easily erodible rock units of the Middle and Lower Jurassic (Figure S2). In contrast, roughly two-thirds of the area of the Danube Swabian Alb tributaries expose Upper Jurassic carbonates, and exposure of Middle and Lower Jurassic rock is confined to incised valleys (Figure S4). The occurrence of Lower and Middle Jurassic rock units correlates strongly with chemical weathering, physical erosion, and hence total denudation rates, which is seen in the Neckar Swabian Alb tributaries (Fig. 4; Table 3). Strong correlation of the chemical weathering rates with the two lithologies may be attributed to Opalinus clay at the base of the Middle Jurassic (Figure S5). This clay is known to be rich in pyrite (e.g., Hinderer, 2006), which enhances chemical weathering by the release of sulfuric acid (e.g., Ross et al., 2018). Additionally, the clay swells and disaggregates when wetted, promoting physical erosion (Thury, 2001). In this view, the steep topography of the escarpment could be coupled to the higher physical and chemical denudation rates of weak bedrock at the base of the escarpment, which facilitates escarpment retreat. Relief across the escarpment and between valleys of the Danube tributaries drives karstification of the Upper Jurassic caprock in both Neckar Swabian Alb tributaries and Danube Swabian Alb tributaries, which show a dominance of chemical weathering, but a two-fold contrast in mean rates across the escarpment.

5.1.3 Connection to escarpment retreat rates

The escarpment retreat rates, calculated using river loads and the basin projection method, range between 1.0 and 9.3 mm/yr (Table 2). These rates are derived from converting vertical denudation into horizontal retreat and are considered maximum values. More specifically, this was done by taking the denudation rate over the catchment area and applying the mass eroded per unit of time across the escarpment height in that catchment. This approach assumes all catchment denudation occurs along the escarpment and provides an upper bound on the retreat rate. However, some measurement sites, such as those for the Kocher and Jagst Rivers, are far away from the Swabian Alb escarpment (Fig. 2). In these cases, since the escarpment constitutes only a minor part of the measured catchments, transforming river load into horizontal retreat rates becomes problematic. For instance, the Kocher and Jagst Rivers, with their large catchments, report retreat rates twice as high as those from smaller catchments near the Swabian Alb escarpment (1.2 to 3.8 mm/yr). Even excluding these higher estimates, the Swabian Alb escarpment's retreat rates are significantly faster than the global average of 0.6 mm/yr (He et al., 2024). These rapid retreat rates are likely due to the contrasting base-level elevations between the Neckar and Danube Rivers (e.g., Villinger,



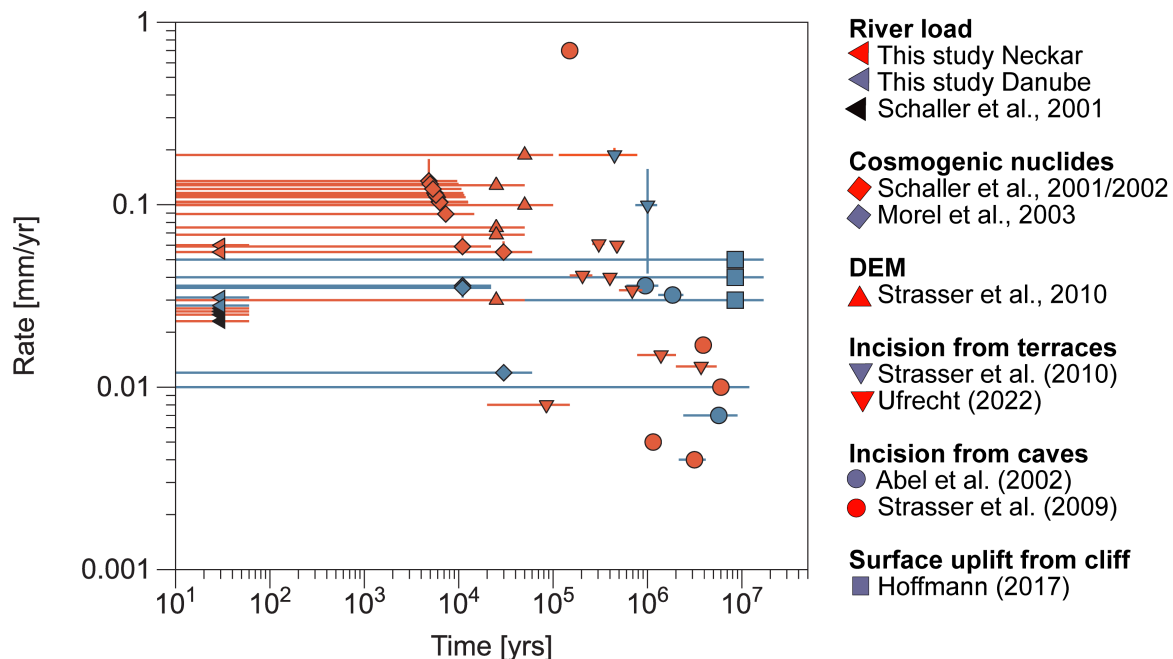
1998; Winterberg and Willett, 2019) and exposure of easily physical and chemically erodible rock units below the Upper Jurassic cap rocks (e.g. Opalinus clay). This lithological contrast and elevation difference affects the geometries of these neighboring river systems, with the Neckar River basin growing as the Danube River basin shrinks.

5.2 Evaluating rates over space and time in the Swabian Alb

395 Despite integrating short-time intervals, the higher decadal-scale rates from the Neckar River and its Swabian Alb tributaries than the Danube River and its Swabian Alb tributaries, as well as the escarpment retreat, are reflected in surface change rates over space and time (Figure 6, Table S10A and B). The decadal-scale total denudation rate (TDR 2) for the Danube Swabian Alb tributaries (Figure 6, blue left-pointing triangles) agrees with millennial-scale rates based on in situ-produced cosmogenic ^{10}Be in the uppermost reaches of the Danube River (Morel et al., 2003; blue diamonds). Comparable millennial-scale rates 400 from a Danube Swabian Alb tributary are calculated from cave and terrace incisions (Abel et al., 2002; blue dots). In addition, the decadal-scale rates agree with uplift rates integrating over the last 17.5 million years (Hoffmann, 2017; blue squares). However, the rates of cave and terrace incisions show local pulses of incision that can exceed rates averaged over million-year timescales or spatial scales of $>10 \text{ km}^2$ watersheds (Fig. 6). For example, an increase in denudation rates is seen at around 3 405 million years as rivers changed their drainage system from the Danube River to the Neckar River, and four pulses of incision are reported from the Laierhöhle cave draining today into the Fils River, a tributary of the Neckar River (Abel et al., 2002; blue dots; Strasser et al., 2009; red dots). Incision pulses 1 to 3 attributed to the Danube River indicate rates of 0.004 to 0.017 mm/yr, while pulse 4 attributed to the Neckar River indicates a rate of 0.700 mm/yr over 0.3 million years in the late Pleistocene. Additionally, an increase in incision rate is reported from terraces of the Kocher River, where rates range from 0.042 to 0.157 mm/yr before 0.78 million years, followed by rates of 0.170 to 0.205 mm/yr at ~ 0.5 million years (Strasser et 410 al., 2010; downward-pointing blue triangles). This transient increase in rates is caused by the capture of the Ur-Kocher (original Kocher River that drained into the Danube River) by the Neckar River (Strasser et al., 2010). These transient pulses of incision are integrated by catchment-averaged denudation rates derived from in situ-produced ^{10}Be concentrations of river sand, which integrate over millennial timescales and typically exceed decadal-scale estimates of denudation from river load.



415 **Figure 6: Temporal synopsis of surface change rates:** Compilation of rates integrating over different timescales for the Neckar-draining side of the Swabian Alb (Red) and the Danube-draining side (Blue). A) Million-year scale uplift rates (Squares). B) Million-year to millennial-scale rates based on incision into cave or terrace markers of known age (Circles and downward-pointing triangles),



420 respectively). C) Millennial-scale rates calculated from DEM analysis (Triangle). D) Millennial-scale denudation rates from in situ-produced cosmogenic nuclides (Diamonds). E) Decadal-scale denudation rates from river load gauging as in this study (Left-pointing triangles).

To summarize, decadal- and millennial-scale rates are more heterogeneous and higher on the Neckar-draining side than the Danube-draining side of the Swabian Alb. In contrast, million-year scale rates on both sides are comparable and in the range of the decadal-scale rates of the Danube Swabian Alb tributaries. The rates over space and time reflect a consistent picture with lower denudation rates from the plateau and increased denudation rates at the escarpment and its foreland due to 425 continuous escarpment retreat and associated river captures.

5.3 Indications from the chemical depletion fraction CDF

Calculated CDFs across the Neckar and Danube Rivers can range from being entirely governed by chemical weathering to being dominated by physical erosion (Figure 7A). All CDFs for the Danube and Neckar Swabian Alb tributaries are higher than 0.45, with averages of 0.92 and 0.78, respectively. This difference is due to higher physical erosion rates in the 430 Neckar River than in the Danube River due to escarpment retreat and river captures (Figure 4B). These high CDF values, which indicate that chemical weathering is the dominant lowering process, are comparable to other German rivers, such as the Weser River (0.99) and the Elbe River (0.95), as well as to the Seine River (0.92) in France (Table S11A). These high values



are common for catchments in low-relief mountain ranges with mainly mixed sedimentary lithologies under temperate climatic conditions. However, they contrast to values from catchments in other lithologies, in more active tectonic settings, or under
435 different climatic conditions (e.g., Gaillardet et al., 1999; West et al., 2005).

A large spread in CDFs is also reported from values based on cosmogenic nuclides for the total denudation and river load for chemical weathering rates (Figure 7B and 7C; Table S11B and C). CDF values from the Apennines, a tectonically active mountain range with mixed lithologies, range from 0 to 1.0 (Erlanger et al. 2021). CDFs reported from tropical Cuba with mixed lithologies and tectonic uplift around 0.02 to 0.11 mm/yr (Muhs et al., 2017), range from 0.3 for igneous rocks to 0.96
440 for sedimentary rocks, respectively (Campbell et al., 2022). In contrast, CDFs from Panama, an active tectonic setting with igneous rocks under a tropical climate, reveal values below 0.4 (Gonzales et al., 2016). Higher CDF values than in Panama are reported for metamorphic crystalline basement rocks in tropical climates such as Sri Lanka (von Blanckenburg et al., 2004) and Cameroon (Regard et al., 2016).

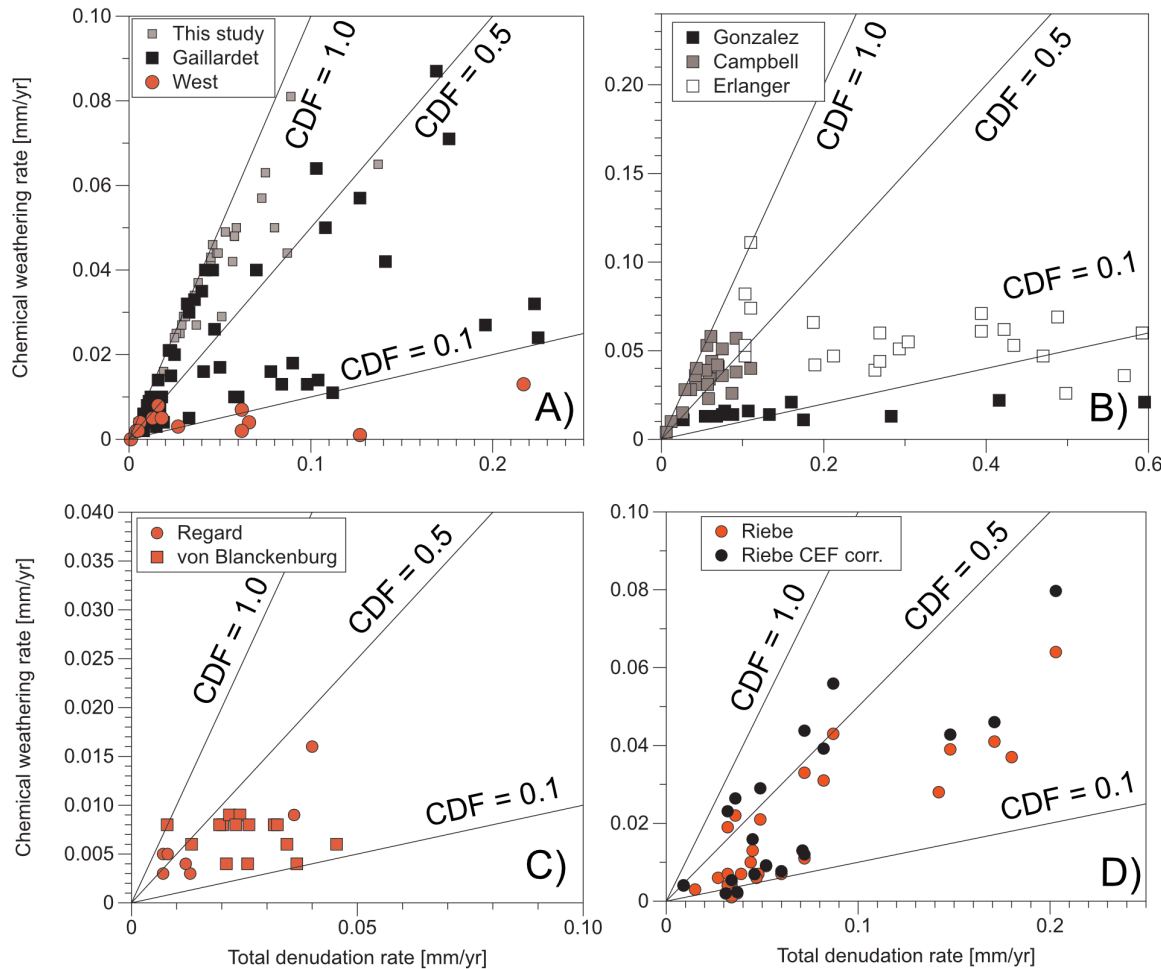


Figure 7: Overview of chemical depletion fractions CDF: Chemical weathering rates versus total denudation rates with lines for chemical depletion fractions (CDF) of 0.1, 0.5, and 1.0. Squares and circles indicate data based on catchments with mixed and dominantly granitoid lithologies, respectively. A) Data based on river load (e.g., Gaillardet et al., 1999; West et al., 2005; and this study); B) Data based on cosmogenic nuclides and river load in mixed lithologies (e.g., Gonzalez et al., 2016; Erlanger et al., 2021; Campbell et al., 2022). C) Data based on cosmogenic nuclides and river load in mainly granitoid lithologies (e.g., von Blanckenburg et al., 2004; Regard et al., 2016). D) Data based on cosmogenic nuclides and immobile elements (Riebe et al., 2004), which has been corrected for the chemical erosion factor CEF after Riebe and Granger (2013).

Compared to other techniques that integrate longer timescales and are more representative of landscape evolution (e.g., Riebe et al., 2004; Riebe and Granger, 2013), catchment river loads integrate chemical weathering and physical erosion across diverse bedrock lithologies and include weathering processes that occur in a deeply karstified environment (e.g., Campbell et al., 2022). However, CDFs derived from river loads can be elevated if physical erosion rates derived from suspended sediment flux are underestimated relative to total sediment fluxes that integrate longer timescales (Pratt-Sitaula et al., 2007). The Neckar and Danube watersheds both include variations in bedrock stratigraphy and deep weathering processes,



and despite the short integration period of river load measurements, calculated denudation rates reflect long-term rates of regional rock uplift and can provide insights into the mechanics of escarpment retreat in packages of layered sedimentary rock.

Climate, as well as tectonics and lithology, have an important influence on chemical weathering rates and CDFs, as reported by Riebe et al. (2004). CDF values (Figure 7D) were calculated based on total denudation from cosmogenic nuclides in river sediment in combination with chemical weathering rates derived from the abundance of immobile elements in soil and rock. In addition, a correction for the total denudation from cosmogenic nuclides due to weathering in regolith was introduced (Riebe and Granger, 2013). The method of cosmogenic nuclides in combination with immobile elements is considered to determine total denudation and chemical weathering rates over a similar timescale. Unfortunately, this method of in situ-produced cosmogenic ^{10}Be in river sediment is restricted to quartz-bearing lithologies. The method of in situ-produced cosmogenic ^{36}Cl can be applied to carbonates for total denudation rates, but still relies on chemical weathering rates from river load (e.g., Ott et al., 2019; Ott et al., 2023). The combination of in situ-produced cosmogenic ^{10}Be and ^{36}Cl in quartz-bearing lithologies allows the determination of total denudation and chemical weathering rates (e.g., Ott et al., 2022). Another promising new tool to determine total denudation and chemical weathering rates over similar timescales in lithologies devoid of quartz (e.g., mafic, ultramafic, and carbonate lithologies; Table S11D) is the method of meteoric ^{10}Be in river load (Willenbring and von Blanckenburg, 2010; Wittmann et al., 2015; Dannhaus et al., 2018; Wittmann et al., 2024). Despite the increasing number of methods allowing the quantification of chemical weathering, physical erosion, and total denudation rates, disentangling the importance of lithology, tectonics, and climate/biota remains still challenging. The same method (e.g., meteoric ^{10}Be) should be applied in several simple natural settings differing in only one factor.

475 6 Conclusions

The denudational imprint of tectonics and lithology in a region with similar climate and biota has been addressed using decadal-scale catchment-wide physical erosion and chemical weathering rates from suspended and dissolved river load in the Swabian Alb (Southwest Germany), indicating:

- 1) Total denudation rates are generally dominated by chemical weathering, with chemical depletion fractions of CDFs as high as 0.97. While the Danube Swabian Alb tributaries are governed by chemical weathering, Neckar Swabian Alb tributaries show higher physical erosion due to escarpment retreat and river capture events. Average total denudation rates, and thus morphological activity from the Neckar Swabian Alb tributaries with their higher relief, are two times higher than rates from the Danube Swabian Alb tributaries. Subsequent estimated retreat rates of the Swabian Alb escarpment range from 1.2 to 9.3 mm/yr.
- 2) Decadal-, millennial- and million-year-scale rates from the Danube-draining side of the Swabian Alb report relatively homogenous surface change rates close to the uplift rate over the last 17.5 Ma. In contrast, millennial- and decadal-scale



denudation rates in the Neckar-draining side are generally up to one order higher than in the Danube-draining side, witnessing ongoing stream capture and escarpment retreat.

3) Comparable chemical depletion fractions (CDFs) from catchments in different lithologic, tectonic, and climatic/biotic
490 settings reported with river load and in situ-produced cosmogenic nuclides reveal a complex interplay of processes. To better understand rates and processes, several simple natural settings differing in only one factor should be investigated with a single method.

Acknowledgement

We thank the „Bundesgesellschaft für Endlagerung“ for supporting this study by grant STAFlE-21-12-Klei. We would like
495 to thank the reviewers for constructive comments.

Data Availability:

The new data presented in this study used for calculation of chemical weathering, physical erosion, and total denudation are available via XXX (www.zenodo.org) [Data will be published upon acceptance of the article]

Author contribution:

500 MS collected the data, wrote text, and made figures with DP. All co-authors wrote specific sections of the manuscript.

Competing interest:

No competing interests exist.

The References

Abel, T., Hinderer, M., and Sauter, Martin: Karst genesis of the Swabian Alb, south Germany, since the Pliocene, Acta
505 Geologica Polonica, 52, 43–54, 2002.

Agster Gottfried: Ein- und Austrag sowie Umsatz gelöster Stoffe in den Einzugsgebieten des Schönbuchs, in: Das
landschaftsökologische Forschungsprojekt Naturpark Schönbuch, VCH, Weinheim, 343–356, n.d.

Ahnert, F.: Functional relationships between denudation, relief, and uplift in large, mid-latitude drainage basins, American
Journal of Science, 268, 243–263, <https://doi.org/10.2475/ajs.268.3.243>, 1970.

510 BGR: Bundesanstalt für Geowissenschaften und Rohstoffe. Geologische Übersichtskarte der Bundesrepublik Deutschland
1:250 000 (GÜK250, WMS), 2019.



von Blanckenburg, F., Hewawasam, T., and Kubik, P. W.: Cosmogenic nuclide evidence for low weathering and denudation in the wet, tropical highlands of Sri Lanka, *J. Geophys. Res.*, 109, F03008, <https://doi.org/10.1029/2003JF000049>, 2004.

515 von Blanckenburg, F., Bouchez, J., and Wittmann, H.: Earth surface erosion and weathering from the ^{10}Be (meteoric)/ ^{9}Be ratio, *Earth and Planetary Science Letters*, 351–352, 295–305, <https://doi.org/10.1016/j.epsl.2012.07.022>, 2012.

Blöthe, J. H. and Hoffmann, T.: Spatio-temporal differences dominate suspended sediment dynamics in medium-sized catchments in central Germany, *Geomorphology*, 418, 108462, <https://doi.org/10.1016/j.geomorph.2022.108462>, 2022.

520 Brown, E. T., Stallard, R. F., Larsen, M. C., Raisbeck, G. M., and Yiou, F.: Denudation rates determined from the accumulation of in situ-produced ^{10}Be in the Luquillo Experimental Forest, Puerto Rico, *Earth and Planetary Science Letters*, 129, 193–202, [https://doi.org/10.1016/0012-821X\(94\)00249-X](https://doi.org/10.1016/0012-821X(94)00249-X), 1995.

Bufe, A., Rugenstein, J. K. C., and Hovius, N.: CO₂ drawdown from weathering is maximized at moderate erosion rates, *Science*, 383, 1075–1080, <https://doi.org/10.1126/science.adk0957>, 2024.

525 Burke, B. C., Heimsath, A. M., and White, A. F.: Coupling chemical weathering with soil production across soil-mantled landscapes, *Earth Surf. Process. Landforms*, 32, 853–873, <https://doi.org/10.1002/esp.1443>, 2007.

Campbell, M. K., Bierman, P. R., Schmidt, A. H., Sibello Hernández, R., García-Moya, A., Corbett, L. B., Hidy, A. J., Cartas Águila, H., Guillén Arruebarrena, A., Balco, G., Dethier, D., and Caffee, M.: Cosmogenic nuclide and solute flux data from central Cuban rivers emphasize the importance of both physical and chemical mass loss from tropical landscapes, *Geochronology*, 4, 435–453, <https://doi.org/10.5194/gchron-4-435-2022>, 2022.

530 Dannhaus, N., Wittmann, H., Krám, P., Christl, M., and Von Blanckenburg, F.: Catchment-wide weathering and erosion rates of mafic, ultramafic, and granitic rock from cosmogenic meteoric $^{10}\text{Be}/^{9}\text{Be}$ ratios, *Geochimica et Cosmochimica Acta*, 222, 618–641, <https://doi.org/10.1016/j.gca.2017.11.005>, 2018.

Davis, W. M.: The Drainage of Cuestas, *Proceedings of the Geologists' Association*, 16, 75–93, [https://doi.org/10.1016/S0016-7878\(99\)80031-5](https://doi.org/10.1016/S0016-7878(99)80031-5), 1899.

535 DGJ: Deutsches Gewässerkundliches Jahrbuch Donaugebiet, Bayerisches Landesamt für Umwelt, 2006.

DGJ: Deutsches Gewässerkundliches Jahrbuch Rheingebiet, Teil I, Landesanstalt für Umweltschutz Baden-Württemberg, 2009.

DiBiase, R. A., Whipple, K. X., Heimsath, A. M., and Ouimet, W. B.: Landscape form and millennial erosion rates in the San Gabriel Mountains, CA, *Earth Planet. Sci. Lett.*, 289, 134–144, <https://doi.org/10.1016/j.epsl.2009.10.036>, 2010.

540 Dietrich, W. E. and Perron, J. T.: The search for a topographic signature of life, *Nature*, 439, 411–418, <https://doi.org/10.1038/nature04452>, 2006.



Dixon, J. L., Heimsath, A. M., and Amundson, R.: The critical role of climate and saprolite weathering in landscape evolution, *Earth Surface Processes and Landforms*, 34, 1507–1521, <https://doi.org/10.1002/esp.1836>, 2009.

Erlanger, E. D., Rugenstein, J. K. C., Bufe, A., Picotti, V., and Willett, S. D.: Controls on Physical and Chemical Denudation
545 in a Mixed Carbonate-Siliciclastic Orogen, *Journal of Geophysical Research: Earth Surface*, 126, e2021JF006064,
<https://doi.org/10.1029/2021JF006064>, 2021.

European Commission Directorate-General Joint Research Centre. Normalised Difference Vegetation Index Statistics 1999-
2019 (raster 1 km), global, 10-daily – version 3.
https://land.copernicus.vgt.vito.be/geonetwork/srv/api/records/urn:ccls:global:ndvi_stats_all.

550 Flint, J. J.: Stream gradient as a function of order, magnitude, and discharge, *Water Resources Research*, 10, 969–973,
<https://doi.org/10.1029/WR010i005p00969>, 1974.

Forte, A. M. and Whipple, K. X.: Short communication: The Topographic Analysis Kit (TAK) for TopoToolbox, *Earth Surf.
Dynam.*, 7, 87–95, <https://doi.org/10.5194/esurf-7-87-2019>, 2019.

Gaillardet, J., Dupré, B., Louvat, P., and Allègre, C. J.: Global silicate weathering and CO₂ consumption rates deduced from
555 the chemistry of large rivers, *Chemical Geology*, 159, 3–30, [https://doi.org/10.1016/S0009-2541\(99\)00031-5](https://doi.org/10.1016/S0009-2541(99)00031-5), 1999.

GKD: Gewässerkundlicher Dienst Bayern, <https://www.gkd.bayern.de/>, last access: 15 January 2023.

Gonzalez, V. S., Bierman, P. R., Nichols, K. K., and Rood, D. H.: Long-term erosion rates of Panamanian drainage basins
determined using in situ 10 Be, *Geomorphology*, 275, 1–15, <https://doi.org/10.1016/j.geomorph.2016.04.025>, 2016.

Granger, D. E., Kirchner, J. W., and Finkel, R.: Spatially Averaged Long-Term Erosion Rates Measured from in Situ-Produced
560 Cosmogenic Nuclides in Alluvial Sediment, *The Journal of Geology*, 104, 249–257, <https://doi.org/10.1086/629823>,
1996.

Harel, M.-A., Mudd, S. M., and Attal, M.: Global analysis of the stream power law parameters based on worldwide 10 Be
denudation rates, *Geomorphology*, 268, 184–196, <https://doi.org/10.1016/j.geomorph.2016.05.035>, 2016.

He, C., Braun, J., Tang, H., Yuan, X., Acevedo-Trejos, E., Ott, R. F., and Stucky De Quay, G.: Drainage divide migration and
565 implications for climate and biodiversity, *Nat Rev Earth Environ*, 5, 177–192, <https://doi.org/10.1038/s43017-023-00511-z>, 2024.

Heimsath, A.M. and Burke, B.: The impact of local geochemical variability on quantifying hillslope soil production and
chemical weathering, *Geomorphology*, 200, 75–88, 2013.

Hewawasam, T.: Increase of human over natural erosion rates in tropical highlands constrained by cosmogenic nuclides,
597–
570 600, [https://doi.org/10.1130/0091-7613\(2003\)031<0597:IOHONE>2.0.CO;2](https://doi.org/10.1130/0091-7613(2003)031<0597:IOHONE>2.0.CO;2), 2003.



Hinderer, M.: Stoffbilanzen in kleinen Einzugsgebieten Baden-Württembergs: Herrn Professor Gerhard Einsele zum 80. Geburtstag gewidmet, Grundwasser, 11, 164–178, <https://doi.org/10.1007/s00767-006-0142-y>, 2006.

Hoffmann Markus: Young tectonic evolution of the Northern Alpine Foreland Basin, southern Germany, based on linking geomorphology and structural geology, Dissertation, Ludwig Maximilian University of Munich, 212 pp., 2017.

575 Hofmann, F., Reichenbacher, B., and Farley, K. A.: Evidence for >5 Ma paleo-exposure of an Eocene–Miocene paleosol of the Bohnerz Formation, Switzerland, Earth and Planetary Science Letters, 465, 168–175, <https://doi.org/10.1016/j.epsl.2017.02.042>, 2017.

Karger, D. N., Conrad, O., Böhner, J., Kawohl, T., Kreft, H., Soria-Auza, R. W., Zimmermann, N. E., Linder, H. P., and Kessler, M.: Climatologies at high resolution for the earth's land surface areas, Scientific Data, 4, sdata2017122, 580 <https://doi.org/10.1038/sdata.2017.122>, 2017.

Karger, D. N., Conrad, O., Böhner, J., Kawohl, T., Kreft, H., Soria-Auza, R. W., Zimmermann, N. E., Linder, H. P., and Kessler, M.: Climatologies at high resolution for the earth's land surface areasCHELSA V2.1 (current) (2.1), <https://doi.org/10.16904/ENVIDAT.228.V2.1>, 2021.

585 Kirby, E. and Whipple, K. X.: Expression of active tectonics in erosional landscapes, Journal of Structural Geology, 44, 54–75, <https://doi.org/10.1016/j.jsg.2012.07.009>, 2012.

Larsen, I. J., Almond, P. C., Eger, A., Stone, J. O., Montgomery, D. R., and Malcolm, B.: Rapid Soil Production and Weathering in the Southern Alps, New Zealand, Science, 343, 637–640, <https://doi.org/10.1126/science.1244908>, 2014.

León-Tavares, J., Roujean, J.-L., Smets, B., Wolters, E., Toté, C., and Swinnen, E.: Correction of Directional Effects in VEGETATION NDVI Time-Series, Remote Sensing, 13, 1130, <https://doi.org/10.3390/rs13061130>, 2021.

590 LGL-BW ATKIS Digitales Geländemodell DGM 5m. Landesamt für Geoinformation und Landentwicklung Baden-Württemberg, 2005.

LUBW: Karten und Datendienst der LUBW: <https://udo.lubw.baden-wuerttemberg.de/public/>, last access: 15 January 2023.

Maher, K. and Chamberlain, C. P.: Hydrologic Regulation of Chemical Weathering and the Geologic Carbon Cycle, Science, 343, 1502–1504, <https://doi.org/10.1126/science.1250770>, 2014.

595 Meybeck, M.: Composition chimique des ruisseaux non pollués en France. Chemical composition of headwater streams in France, sgeol, 39, 3–77, <https://doi.org/10.3406/sgeol.1986.1719>, 1986.

Montgomery, D. R. and Brandon, M. T.: Topographic controls on erosion rates in tectonically active mountain ranges, Earth and Planetary Science Letters, 201, 481–489, [https://doi.org/10.1016/S0012-821X\(02\)00725-2](https://doi.org/10.1016/S0012-821X(02)00725-2), 2002.



- Morel, P., Von Blanckenburg, F., Schaller, M., Kubik, P. W., and Hinderer, M.: Lithology, landscape dissection and glaciation
600 controls on catchment erosion as determined by cosmogenic nuclides in river sediment (the Wutach Gorge, Black Forest), *Terra Nova*, 15, 398–404, <https://doi.org/10.1046/j.1365-3121.2003.00519.x>, 2003.
- Muhs, D. R., Schweig, E. S., Simmons, K. R., and Halley, R. B.: Late Quaternary uplift along the North America-Caribbean plate boundary: Evidence from the sea level record of Guantanamo Bay, Cuba, *Quaternary Science Reviews*, 178, 54–76, <https://doi.org/10.1016/j.quascirev.2017.10.024>, 2017.
- Ott, R. F., Gallen, S. F., Caves Rugenstein, J. K., Ivy-Ochs, S., Helman, D., Fassoulas, C., Vockenhuber, C., Christl, M., and Willett, S. D.: Chemical Versus Mechanical Denudation in Meta-Clastic and Carbonate Bedrock Catchments on Crete, Greece, and Mechanisms for Steep and High Carbonate Topography, *Journal of Geophysical Research: Earth Surface*, 124, 2943–2961, <https://doi.org/10.1029/2019JF005142>, 2019.
- Ott, R. F., Gallen, S. F., and Granger, D. E.: Cosmogenic nuclide weathering biases: Corrections and potential for denudation
610 and weathering rate measurements, *Cosmogenic nuclide dating*, <https://doi.org/10.5194/gchron-2022-5>, 2022.
- Ott, R. F., Gallen, S. F., and Helman, D.: Erosion and weathering in carbonate regions reveal climatic and tectonic drivers of carbonate landscape evolution, <https://doi.org/10.5194/egusphere-2022-1376>, 3 January 2023.
- Peifer, D., Persano, C., Hurst, M. D., Bishop, P., and Fabel, D.: Growing topography due to contrasting rock types in a tectonically dead landscape, *Earth Surface Dynamics*, 9, 167–181, <https://doi.org/10.5194/esurf-9-167-2021>, 2021.
- Petit, C., Campy, M., Chaline, J., and Bonvalot, J.: Major palaeohydrographic changes in Alpine foreland during the Pliocene - Pleistocene, *Boreas*, 25, 131–143, <https://doi.org/10.1111/j.1502-3885.1996.tb00841.x>, 1996.
- Portenga, E. W. and Bierman, P. R.: Understanding Earth's eroding surface with ^{10}Be , *GSA Today*, 21, 4–10, <https://doi.org/10.1130/G111A.1>, 2011.
- Pratt-Sitaula, B., Garde, M., Burbank, D. W., Oskin, M., Heimsath, A., and Gabet, E.: Bedload-to-suspended load ratio and
620 rapid bedrock incision from Himalayan Landslide-dam lake record, *Quat. res.*, 68, 111–120, <https://doi.org/10.1016/j.yqres.2007.03.005>, 2007.
- Raymo, M. E., Ruddiman, W. F., and Froelich, P. N.: Influence of late Cenozoic mountain building on ocean geochemical cycles, *Geol.*, 16, 649, [https://doi.org/10.1130/0091-7613\(1988\)016<0649:IOLCMB>2.3.CO;2](https://doi.org/10.1130/0091-7613(1988)016<0649:IOLCMB>2.3.CO;2), 1988.
- Regard, V., Carretier, S., Boeglin, J., Ndam Ngoupayou, J., Dzana, J., Bedimo Bedimo, J., Riotte, J., and Braun, J.: Denudation
625 rates on cratonic landscapes: comparison between suspended and dissolved fluxes, and ^{10}Be analysis in the Nyong and Sanaga River basins, south Cameroon, *Earth Surf Processes Landf.*, 41, 1671–1683, <https://doi.org/10.1002/esp.3939>, 2016.



- Riebe, C. S. and Granger, D. E.: Quantifying effects of deep and near-surface chemical erosion on cosmogenic nuclides in soils, saprolite, and sediment: EFFECTS OF CHEMICAL EROSION ON COSMOGENIC NUCLIDE BUILDUP, 630 Earth Surf. Process. Landforms, 38, 523–533, <https://doi.org/10.1002/esp.3339>, 2013.
- Riebe, C. S., Kirchner, J. W., and Finkel, R. C.: Erosional and climatic effects on long-term chemical weathering rates in granitic landscapes spanning diverse climate regimes, Earth and Planetary Science Letters, 224, 547–562, <https://doi.org/10.1016/j.epsl.2004.05.019>, 2004.
- Ring, U. and Bolhar, R.: Tilting, uplift, volcanism and disintegration of the South German block, Tectonophysics, 795, 228611, 635 <https://doi.org/10.1016/j.tecto.2020.228611>, 2020.
- Ross, M. R. V., Nippgen, F., Hassett, B. A., McGlynn, B. L., and Bernhardt, E. S.: Pyrite Oxidation Drives Exceptionally High Weathering Rates and Geologic CO₂ Release in Mountaintop-Mined Landscapes, Global Biogeochemical Cycles, 32, 1182–1194, <https://doi.org/10.1029/2017GB005798>, 2018.
- Ryb, U., Matmon, A., Erel, Y., Haviv, I., Benedetti, L., and Hidy, A. J.: Styles and rates of long-term denudation in carbonate terrains under a Mediterranean to hyper-arid climatic gradient, Earth and Planetary Science Letters, 406, 142–152, 640 <https://doi.org/10.1016/j.epsl.2014.09.008>, 2014.
- Schaller, M. and Ehlers, T. A.: Comparison of soil production, chemical weathering, and physical erosion rates along a climate and ecological gradient (Chile) to global observations, Earth Surf. Dynam., 10, 131–150, <https://doi.org/10.5194/esurf-10-131-2022>, 2022.
- Schaller, M., von Blanckenburg, F., Hovius, N., and Kubik, P. W.: Large-scale erosion rates from in situ-produced cosmogenic nuclides in European river sediments, Earth and Planetary Science Letters, 188, 441–458, 645 [https://doi.org/10.1016/S0012-821X\(01\)00320-X](https://doi.org/10.1016/S0012-821X(01)00320-X), 2001.
- Schaller, M., von Blanckenburg, F., Veldkamp, A., Tebbens, L. A., Hovius, N., and Kubik, P. W.: A 30 000 yr record of erosion rates from cosmogenic ¹⁰Be in Middle European river terraces, Earth and Planetary Science Letters, 204, 307–320, 650 [https://doi.org/10.1016/S0012-821X\(02\)00951-2](https://doi.org/10.1016/S0012-821X(02)00951-2), 2002.
- Schwanghart, W. and Scherler, D.: Short Communication: TopoToolbox 2 – MATLAB-based software for topographic analysis and modeling in Earth surface sciences, Earth Surface Dynamics, 2, 1–7, <https://doi.org/10.5194/esurf-2-1-2014>, 2014.
- Strasser, A., Strasser, M., and Seyfried, H.: Quantifying erosion over timescales of one million years: A photogrammetric approach on the amount of Rhenish erosion in southwestern Germany, Geomorphology, 122, 244–253, 655 <https://doi.org/10.1016/j.geomorph.2009.06.027>, 2010.



Strasser, M., Strasser, A., Pelz, K., and Seyfried, H.: A mid Miocene to early Pleistocene multi-level cave as a gauge for tectonic uplift of the Swabian Alb (Southwest Germany), *Geomorphology*, 106, 130–141, <https://doi.org/10.1016/j.geomorph.2008.09.012>, 2009.

660 Terhorst, B.: Mass movements of various ages on the Swabian Jurassic escarpment: geomorphologic processes and their causes, *Zeitschrift für Geomorphologie N.F.*, 125, 65–87, 2001.

Thury, M.: The characteristics of the Opalinus Clay investigated in the Mont Terri underground rock laboratory in Switzerland, *Comptes Rendus. Physique*, 3, 923–933, [https://doi.org/10.1016/S1631-0705\(02\)01372-5](https://doi.org/10.1016/S1631-0705(02)01372-5), 2002.

665 Turowski, J. M., Rickenmann, D., and Dadson, S. J.: The partitioning of the total sediment load of a river into suspended load and bedload: a review of empirical data: The partitioning of sediment load, *Sedimentology*, 57, 1126–1146, <https://doi.org/10.1111/j.1365-3091.2009.01140.x>, 2010.

Ufrecht, W.: Abfolge und Alter der Neckar-Terrassen und Travertine in Stuttgart (Cannstatter Becken und Nesenbachthal), Jahreshefte der Gesellschaft für Naturkunde in Württemberg, Bd. 178, 253-324 Seiten, <https://doi.org/10.26251/JHGFN.178.2022.253-324>, 2022.

670 Ufrecht, W., Bohnert, J., and Jantschke, H.: Ein konzeptionelles Modell der Verkarstungsgeschichte für das Einzugsgebiet des Blautopfs (mittlere Schwäbische Alb), *Laichinger Höhlenfreund*, 51, 3–44, 2016.

Vanacker, V., von Blanckenburg, F., Govers, G., Molina, A., Poesen, J., Deckers, J., and Kubik, P.: Restoring dense vegetation can slow mountain erosion to near natural benchmark levels, *Geology*, 35, 303–306, <https://doi.org/10.1130/G23109A.1>, 2007.

675 VanLandingham, L. A., Portenga, E. W., Lefroy, E. C., Schmidt, A. H., Bierman, P. R., and Hidy, A. J.: Comparison of basin-scale in situ and meteoric $\text{^{10}Be}$ erosion and denudation rates in felsic lithologies across an elevation gradient at the George River, northeast Tasmania, Australia, *Geochronology*, 4, 153–176, <https://doi.org/10.5194/gchron-4-153-2022>, 2022.

680 Villinger, E.: Zur Flussgeschichte von Rhein und Donau in Südwestdeutschland, *jber_oberrh*, 80, 361–398, <https://doi.org/10.1127/jmogv/80/1998/361>, 1998.

Wang, Y. and Willett, S. D.: Escarpment retreat rates derived from detrital cosmogenic nuclide concentrations, *Earth Surf. Dynam.*, 9, 1301–1322, <https://doi.org/10.5194/esurf-9-1301-2021>, 2021.

685 Wang, Y., Willett, S. D., Wu, D., Haghipour, N., and Christl, M.: Retreat of the Great Escarpment of Madagascar From Geomorphic Analysis and Cosmogenic ^{10}Be Concentrations, *Geochem Geophys Geosyst*, 22, e2021GC009979, <https://doi.org/10.1029/2021GC009979>, 2021.



West, A., Galy, A., and Bickle, M.: Tectonic and climatic controls on silicate weathering, *Earth and Planetary Science Letters*, 235, 211–228, <https://doi.org/10.1016/j.epsl.2005.03.020>, 2005.

Whipple, K. X. and Tucker, G. E.: Dynamics of the stream-power river incision model: Implications for height limits of mountain ranges, landscape response timescales, and research needs, *Journal of Geophysical Research: Solid Earth*, 104, 17661–17674, <https://doi.org/10.1029/1999JB900120>, 1999.
690

Willenbring, J. K. and von Blanckenburg, F.: Long-term stability of global erosion rates and weathering during late-Cenozoic cooling, *Nature*, 465, 211–214, <https://doi.org/10.1038/nature09044>, 2010.

Winterberg, S. and Willett, S. D.: Greater Alpine river network evolution, interpretations based on novel drainage analysis, *Swiss J Geosci*, 112, 3–22, <https://doi.org/10.1007/s00015-018-0332-5>, 2019.

695 Wittmann, H., Von Blanckenburg, F., Dannhaus, N., Bouchez, J., Gaillardet, J., Guyot, J. L., Maurice, L., Roig, H., Filizola, N., and Christl, M.: A test of the cosmogenic ^{10}Be (meteoric)/ ^{9}Be proxy for simultaneously determining basin-wide erosion rates, denudation rates, and the degree of weathering in the Amazon basin: EROSION FROM METEORIC $^{10}\text{BE}/^{9}\text{BE}$ IN AMAZON, *J. Geophys. Res. Earth Surf.*, 120, 2498–2528, <https://doi.org/10.1002/2015JF003581>, 2015.

Wittmann, H., Bouchez, J., Calmels, D., Gaillardet, J., Frick, D., Stroncik, N., ASTER Team, and von Blanckenburg, F.:
700 Denudation and weathering rates of carbonate landscapes from meteoric $^{10}\text{Be}/^{9}\text{Be}$ ratios, <https://doi.org/10.5880/GFZ.3.3.2024.001>, 2024.

Ziegler, P. A. and Fraefel, M.: Response of drainage systems to Neogene evolution of the Jura fold-thrust belt and Upper Rhine Graben, *Swiss J. Geosci.*, 102, 57–75, <https://doi.org/10.1007/s00015-009-1306-4>, 2009.